Carbon 124 (2017) 1–8

Contents lists available at ScienceDirect

Carbon

journal homepage: www.elsevier.com/locate/carbon

Statistical analysis of the temperature dependence of the phonon properties in supported CVD graphene

Jarosław Judek*, Arkadiusz P. Gertych, Maciej Krajewski, Karolina Czerniak, Anna Łapińska, Jan Sobieski, Mariusz Zdrojek

Faculty of Physics, Warsaw University of Technology, Koszykowa 75, 00-662 Warszawa, Poland

ARTICLE INFO

Article history:
Received 21 April 2017
Received in revised form
17 July 2017
Accepted 15 August 2017

ABSTRACT

Existing literature reports on the dependence of phonon properties on temperature rarely use statistical analysis. The lack of uncertainty assessment, which takes into account changes in the parameter value within the sample, substantially hinders comparison among the data reported so far. Moreover, it is impossible to determine whether these results display discrepancies between themselves due to sample- and technology-dependent issues, manifestations of statistical noise, or a deeper cause that has not yet been grasped. Here, we show the distributions of the phonon properties at temperatures in the range of 300 K–500 K, which were used to calculate the temperature derivatives of the phonon energies χ. These can be used in the procedure of the extraction of graphene thermal conductivity κ but are also related to the anharmonic part of the graphene crystal lattice potential and/or nonadiabatic effects. Finally, we show that the correlation analyses revealed the existence of an unknown physical cause of differences between χ values, showing that the thermal properties of phonons in graphene are still not fully understood and further studies on the contribution of doping, stress, defects and interaction with the substrate, including its thermal expansion, are required to explain the observed parameter variability.

1. Introduction

Today, eight years after the first reports in the literature [1–3], large-scale graphene production on copper foil using Chemical Vapor Deposition (CVD), the only process that meets industrial requirements, is still not mature. Thus, CVD graphene, in contrast to the exfoliated material, is an inhomogeneous and non-ideal material. Typical SEM images of graphene grown on copper foil and transferred onto a typical Si/SiO_2 substrate using the delamination method [4] are shown in Fig. 1. Grain boundaries, second layer seeds, wrinkles, and cracks are only examples of the commonly occurring defects. Therefore, it is intuitive that parameters characterizing such a monolayer related to, e.g., electron [5–7] or phonon properties [8–10], should not be described by single values but rather by distributions. These, characterized by a scope of variation usually much higher than the uncertainty of a single measurement, will reflect the fluctuation of the investigated parameters within the sample; thus, they could be treated as technology quality indicators. Another advantage of having a consistent set of data is the access to correlation analysis, which is able to reveal the physical source of the parameter variability, often giving key interpretations or providing useful features. It was shown, for example, that analysis of the correlations between the energies of different phonons in graphene enables optical separation of the stress and doping level [11] or provides an estimation of the stress variation on the nanometer scale [12], which is suspected to limit the mobility in graphene electrical devices [13,14].

Existing literature reports on the dependence of the phonon energies $\hbar\omega$ on temperature T [15–30] rarely use statistical analysis while discussing the presented results. The lack of the uncertainty assessment, which takes into account changes in the parameter value within the sample, substantially hinders comparison among data reported by different authors. Moreover, it is impossible to determine whether these results display significant discrepancies between themselves due to the sample- and technology-dependent issues, manifestations of statistical noise, or a deeper cause that has not yet been grasped. On the other hand, reports containing statistical/correlation analyses [11,12] neglect the influence of temperature – another factor, apart from stress and doping, with the ability to significantly affect phonon properties in

* Corresponding author.
E-mail address: jerryj@if.pw.edu.pl (J. Judek).

http://dx.doi.org/10.1016/j.carbon.2017.08.029
0008-6223/

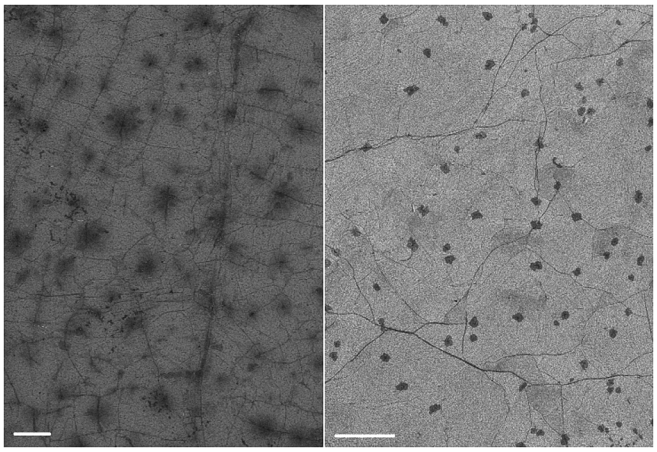

Fig. 1. Typical SEM pictures of CVD graphene monolayers grown on copper foil and transferred onto a typical Si/SiO_2 substrate. Left: homemade sample, length of the white bar equals 2 μm; right: commercially available sample from Graphenea Inc., length of the white bar equals 10 μm.

graphene. This is especially important because the experimental technique, Raman spectroscopy, requires illumination with laser light, which typically leads to an inhomogeneous temperature increase within the spot from which data are collected.

In this paper, we fill the gaps identified above. Using a Raman mapping technique, we obtained distributions of the phonon properties at different temperatures in the range of 300 K–500 K, which were used *inter alia* to calculate the temperature derivatives of the phonon energies $\chi_T = \partial\hbar\omega/\partial T$. These not only can be used in the procedure of the extraction of graphene thermal conductivity κ and interface conductance g [31–34] but also have a purely scientific meaning related to the anharmonic part of the graphene crystal lattice potential and/or nonadiabatic effects. Based on the statistical/correlation analyses, we concluded that temperature and stress, including that from the thermal expansion of the substrate, can have similar and comparable contributions to the phonon energies in supported CVD graphene, which impedes the reliable separation of these factors. Moreover, we demonstrate that the variations in temperature derivatives of the phonon energies are correlated, which means that there is a specific cause for their divergence.

2. Methods

A graphene monolayer was grown on an 18-μm-thick Jtchte Gould copper substrate in an Aixtron Black Magic Pro system from CH_4 as a precursor, aided by the use of Ar and H_2 gases. After growth, the graphene was transferred onto a typical Si/SiO_2 (525 μm thick Si and 285 nm thick SiO_2) substrate using a high-speed delamination method [4]. We also used commercially available samples from Graphenea Inc. for comparison purposes to exclude any technology-dependent issues.

Phonon properties were examined using a Raman mapping technique [35], a variation of Raman spectroscopy that yields the spatial distribution of the Raman spectra for a specified area of the sample, called Raman maps. Such results can be used for visualization of the changes in a material property related to Raman spectrum within a sample, which itself is an interesting capability. However, in this paper, the acquired Raman maps are intended for statistical analysis. Every Raman spectrum from the Raman map is a subject of numerical analysis in order to obtain the values of the G and 2D mode peak positions $\hbar\omega$ (related to phonon energies), widths Γ (primary related to phonon lifetimes), intensities I (related to the inelastic scattering amplitude), and subsequently, the derivatives of the peak positions with respect to the temperature $\chi_T = \partial\hbar\omega/\partial T$. The derivative has interesting interpretation because it can be expressed as [36]:

$$\chi_T = \left(\frac{\partial\hbar\omega}{\partial T}\right)_V + \left(\frac{\partial V}{\partial T}\right)_P \cdot \left(\frac{\partial\hbar\omega}{\partial V}\right)_T.$$

This enables study on the interplay between the purely anharmonic effects and the thermal lattice expansion, which, in this approach, is responsible for the change in the force constant values. All considered distributions comprise the corresponding above described 'point' data. Typical 'point' Raman spectra are shown in Fig. 2. Two peaks called G and 2D can be observed; both are well described by the Lorentzian function. No D mode is observed in our samples, which denotes low defect concentration. The I_{2D}/I_G ratio equals approximately 3.5, which proves that our samples are high quality.

3. Results and discussion

3.1. Stability tests

All Raman measurements were taken under ambient atmosphere, in an environment characterized by the presence of moisture and oxygen molecules, which are known graphene hole dopants [37,38] and oxidizing agents in the presence of light [39]. Both facts are very important and immediately entail discussion of the impact of the laser light illumination, an inherent element of Raman measurement, on the reliability of the obtained results. Our doubts arise from the literature reports of substrate-dependent optical doping in supported graphene [40] and/or its photo(-thermal) oxidation during laser irradiation [41–44]. The latter process might occur even at laser power densities often assumed to be safe [45]. Both phenomena might lead to significant shifts of the G and 2D mode peak positions in consecutive Raman spectra when making a series of measurements at the same position. In consequence, they potentially affect the value of the derivative of the mode position with respect to the temperature, which requires at least a few experimental points. Therefore, before studying the graphene thermal properties, we performed a stability test, the main results of which are illustrated in Fig. 3. We note that presented data are highly sample- and technology-dependent and are intended only to briefly illustrate the problem of graphene stability and to demonstrate the proper handling of this problem in our work.

Fig. 3 consists of six traces in the main part and two data sets in the inset. The values of the G and 2D peak positions were obtained from 121 consecutive Raman measurements performed at the same position, except for traces (a) and (b), when 484 measurements

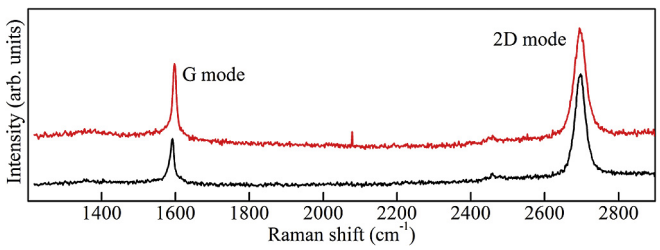

Fig. 2. Representative Raman spectra of a CVD graphene monolayer grown on copper foil and transferred onto a typical Si/SiO_2 substrate. The black solid line corresponds to the sample that we synthesized, while the red solid line corresponds to the commercially available sample from Graphenea Inc. (A colour version of this figure can be viewed online.)

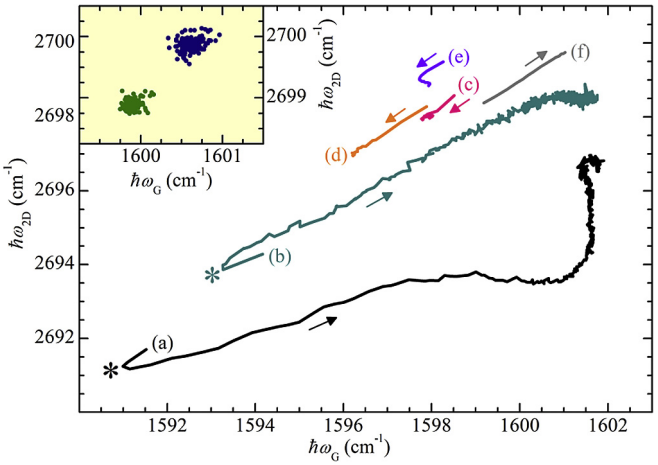

Fig. 3. Time evolution of the G and 2D mode positions for different samples, positions within a sample, laser power density and the pre-treatment procedures. Details are included in the main text. (A colour version of this figure can be viewed online.)

were performed in order to show the scope of possible changes. The G and 2D mode peak positions are visualized in the $\hbar\omega_G$–$\hbar\omega_{2D}$ coordinate system, which is convenient when considering temperature/doping/stress contributions to Raman spectra (after Lee [11], Tiberj [40] and Herziger [43]). Traces (a) and (b) were obtained at two different positions on a *fresh* sample (just after the production process). The laser power P_L focused on the sample by the 50x objective with $NA = 0.50$ equals 1 mW. Observed changes in the G mode position reach 10 cm^{-1}, and the initial part of both traces (symbol * in Fig. 3) often forms a kink. Our results are similar to the results obtained by Herziger [43], except that the direction of the kink is position dependent.

Traces (c)-(f) were obtained on samples that were kept under ambient atmosphere for a few days. The initial values of the G and 2D mode peak positions are higher than those for *fresh* samples, and the scale of changes due to laser irradiation is much smaller. Traces (c) and (d) were obtained when graphene was illuminated by the laser beam focused on the sample with $P_L = 6$ mW. Traces (e) and (f) were obtained when graphene was illuminated by the defocused laser beam (with a diameter of approximately 2 μm) with $P_L = 6$ mW. The values of the G and 2D mode positions can both monotonically increase or decrease and the curve can form a kink, depending on the Raman measurement details.

After annealing under ambient atmosphere at 460 K for 30 min, the initial value of the peak positions of the G and 2D modes increased again, and the stability further improved. However, no changes in phonon energies during irradiation were observed for the defocused laser beam and only for part of the samples. Exemplary data obtained from consecutive measurements at two different positions of the annealed sample with the defocused laser beam for when the CVD graphene monolayer was stable under laser irradiation are shown in the inset in Fig. 3. No time evolution can be observed; the data have a Gaussian-like distribution. The standard deviations of the peak positions of the G and 2D modes are identical and equal to 0.12 cm^{-1} for the first position and 0.082 cm^{-1} for the second position. Because all our measurements were performed in one spectral window with otherwise unchanged spectrometer settings, we estimated that the A-type uncertainty [46] for both the G and 2D mode peak positions equals approximately 0.1 cm^{-1}. The corresponding value of the A-type uncertainty for G and 2D mode peak widths was assumed to equal 0.3 cm^{-1}. We note that the experimentally determined value of the uncertainty does not change in temperature (is constant in the 300 K–500 K temperature range) and it includes particularly following contributions: fluctuations of the laser power (which was estimated to be approximately 0.3% in a 1-h-timescale), fluctuations of the focus position in respect to the sample surface, fluctuations of the temperature of the sample, noise of the CCD, and numerical noise related to the fitting procedure.

The results discussed above are consistent with the work of Lee [11] concerning the changes in the Raman G and 2D mode peak position values versus the temperature of the annealing process, the work of Tiberj [40] concerning the different sensitivities of the samples to optical doping, and the work of Amato [45] regarding the statement that, in the case of CVD graphene, even low laser power densities can lead to nonreversible structural changes. Our results are contrary to the results obtained by Costa, who found that changes in the doping are the dominant reason for shifts in the Raman modes [30].

3.2. Temperature studies

Temperature studies were performed on two separate CVD graphene monolayer samples: one commercially available, denoted as S1, and one that we synthesized, denoted as S2. Both samples were annealed just before the measurements (S1 460 K, S2 500 K). The obtained results are reversible with respect to the temperature, and after the heating-cooling cycles, we do not observe significant changes in the D mode intensity (no distinct D mode), in the I_{2D}/I_G ratio (~3.5) or in the average mode positions. We note that our results are contrary to part of the results already published [20,22–24,27,30], which showed differences between the first and next heating-cooling cycles. Based on the results of the stability tests, we used only the defocused laser beam characterized by a diameter of approximately 2 μm and a power of 6 mW in the temperature studies. The Raman mapping involved 121 measurements performed on a 20 μm × 20 μm square area with a 2 μm step. For sample S2, we additionally recorded four Raman maps for each temperature in four corners of the sample that were located approximately 4 mm from each other to see if our map was large enough and whether our data were representative. For every temperature, all four sets did not differ from each other within the uncertainty limit. Thus, we pooled the results for each temperature together to obtain better statistics. The results for samples S1 and S2 do not differ quantitatively, so we focus only on results from sample S2 due to a larger data set (484 experimental points) in the further part of our work.

Fig. 4 shows the main (raw) results of this work, i.e., the distributions of the positions of the G mode $\hbar\omega_G$, distributions of the positions of the 2D mode $\hbar\omega_{2D}$, distributions of the widths of the G mode Γ_G, and distributions of the widths of the 2D mode Γ_{2D}, for five temperature values: 300 K, 350 K, 400 K, 450 K, and 500 K. The results are presented in the form of histograms in Fig. 4a–d, and separately in Fig. 4e–h in $\hbar\omega_{2D}$–$\hbar\omega_G$, Γ_G–$\hbar\omega_G$, Γ_{2D}–$\hbar\omega_{2D}$, and Γ_{2D}–Γ_G coordinate systems, which is convenient while identifying correlations between sets of variables.

The histograms of the G and 2D mode positions and widths (Fig. 4a–d) demonstrate that the obtained data follow normal distributions. Calculated values of the arithmetic mean $\overline{\hbar\omega}$ and standard deviation $\sigma_{\hbar\omega}$ are listed in Table 1. The mean values of the G and 2D mode positions, $\overline{\hbar\omega_G}$ and $\overline{\hbar\omega_{2D}}$, decrease linearly with temperature, as expected. The mean values of the G and 2D mode widths, $\overline{\Gamma_G}$ and $\overline{\Gamma_{2D}}$, increase with temperature, also as expected. The derivative of the mean value of the G mode position with respect to temperature equals:

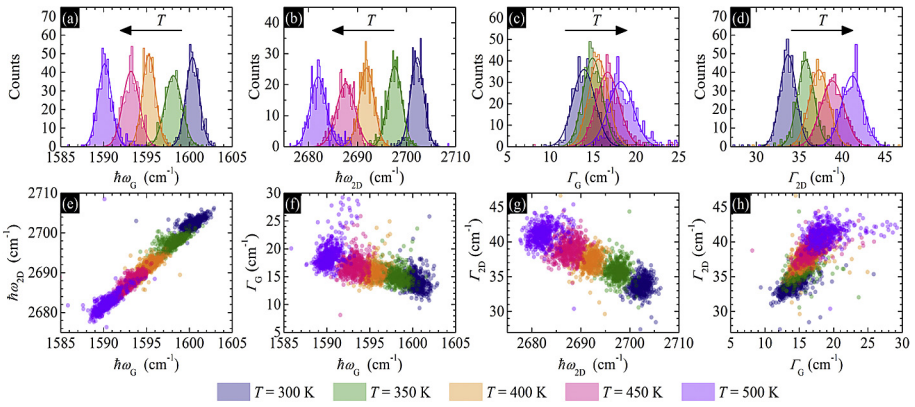

Fig. 4. (a) Histogram of the G mode peak positions; (b) histogram of the 2D mode peak positions; (c) histogram of the G mode peak widths; (d) histogram of the 2D mode peak widths; (e) the 2D mode peak position versus the G mode peak position; (f) the G mode peak width versus the G mode peak position; (g) the 2D mode peak width versus the 2D mode peak position; (h) the 2D mode peak width versus the G mode peak width. Data sets were collected for five temperature values: $T = 300$ K, 350 K, 400 K, 450 K, and 500 K. (A colour version of this figure can be viewed online.)

Table 1
Mean values and standard deviations of the G and 2D peak positions and widths for the data in Fig. 4a–d. Pearson correlation coefficients ρ and derivatives were obtained using Deming orthogonal regression for the data in Fig. 4e and h.

T (K)	$\hbar\omega_G \pm \sigma_{\hbar\omega,G}$ (cm^{-1})	$\hbar\omega_{2D} \pm \sigma_{\hbar\omega,2D}$ (cm^{-1})	$\Gamma_G \pm \sigma_{\Gamma,G}$ (cm^{-1})	$\Gamma_{2D} \pm \sigma_{\Gamma,2D}$ (cm^{-1})	$\rho(\hbar\omega_{2D}, \hbar\omega_G)$	$\partial\hbar\omega_{2D}/\partial\hbar\omega_G$	$\rho(\Gamma_{2D}, \Gamma_G)$	$\partial\Gamma_{2D}/\partial\Gamma_G$
300	1600.4 ± 0.8	2702.2 ± 1.3	14.1 ± 1.4	33.8 ± 1.0	0.70	1.97	0.64	0.63
350	1598.1 ± 1.0	2697.4 ± 1.6	15.1 ± 1.2	35.8 ± 1.1	0.70	1.86	0.57	0.92
400	1595.3 ± 0.8	2691.8 ± 1.5	15.8 ± 1.3	37.4 ± 1.1	0.67	2.57	0.54	0.84
450	1593.2 ± 0.9	2687.4 ± 1.9	16.9 ± 1.5	38.9 ± 1.4	0.81	2.34	0.59	0.89
500	1590.2 ± 0.8	2681.9 ± 1.6	18.4 ± 1.4	41.1 ± 1.2	0.79	2.27	0.28	0.61

$$\chi_{T,G} = \partial\overline{\hbar\omega_G}\Big/\partial T = -0.051\pm0.005\ \mathrm{cm}^{-1}\Big/\mathrm{K}, \quad (1)$$

the derivative of the mean value of the 2D mode position with respect to temperature equals:

$$\chi_{T,2D} = \partial\overline{\hbar\omega_{2D}}\Big/\partial T = -0.101\pm0.009\ \mathrm{cm}^{-1}\Big/\mathrm{K}, \quad (2)$$

the derivative of the mean value of the G mode width with respect to temperature equals:

$$\partial\overline{\Gamma_G}\Big/\partial T = 0.021\pm0.009\ \mathrm{cm}^{-1}\Big/\mathrm{K}, \quad (3)$$

and the derivative of the mean value of the 2D mode width with respect to temperature equals:

$$\partial\overline{\Gamma_{2D}}\Big/\partial T = 0.035\pm0.007\ \mathrm{cm}^{-1}\Big/\mathrm{K}. \quad (4)$$

The values of the derivatives are in good agreement with other studies in the literature, which will be discussed further separately. It is surprising that the values of the uncertainties are relatively high. This occurs because our calculations of the covariance matrix take into account the uncertainties of the raw experimental data, which represents an advisable but rarely employed approach [47]. Uncertainties of the G and 2D mode mean positions and widths are taken as the standard deviations of the corresponding distributions, which is a standard procedure. We note that the values of $\sigma_{\hbar\omega,G}$ and $\sigma_{\hbar\omega,2D}$, as well as the values of $\sigma_{\Gamma,G}$ and $\sigma_{\Gamma,2D}$, are higher than the corresponding uncertainties of a single measurement, which were assumed previously to equal 0.1 cm^{-1} in the case of mode position and 0.3 cm^{-1} in the case of mode width. This means that the divergence of the values of the mode positions and widths comes mostly from the inhomogeneity of the graphene monolayer. We also note that it seems that the values of the standard deviations of the G and 2D mode positions and widths are insensitive to temperature. The assumption that, indeed, $\partial\sigma(T)/\partial T = 0$ implies a conditional conclusion that if there is a specific cause of the divergence of the G and 2D mode positions and widths, this cause is insensitive to the temperature changes.

Fig. 4e–h were used for identifying correlations between phonon properties related to the Raman spectra acquired at constant temperature. A distinct dependence between the G and 2D mode positions and between the G and 2D mode widths can be seen in Fig. 4e and h, respectively. The values of the Pearson correlation coefficients ρ, a quantity that is a measure of the linear dependence of two variables, for both data sets are listed in Table 1. We note that $\rho \geq 0.67$ for mode positions for all temperatures and $\rho \geq 0.54$ for mode widths for all temperatures except the highest one, which justifies our previous finding. On the other hand, the results presented in Fig. 4f and g do not allow us to conclude that there is any dependence between mode position and width either in the case of the G or 2D mode.

Fig. 4e and h illustrate the dependence of $\hbar\omega_{2D}$ on $\hbar\omega_G$ and Γ_{2D} on Γ_G, respectively, at five different temperatures of the substrate. For each temperature, we found the derivative of $\hbar\omega_{2D}$ with respect to $\hbar\omega_G$ and of Γ_{2D} with respect to Γ_G. The results are shown in Table 1. In our calculations, we assumed the linear dependence between the investigated quantities, which technically was equivalent to the search of the slope of a line. For this purpose, we employed the Deming orthogonal regression method [48], which assumes that the uncertainties of both dependent and independent variables are equal, which exactly matches our case. The average over the temperature value of the derivative of the 2D mode position with respect to the G mode position equals:

$$\partial\hbar\omega_{2D}/\partial\hbar\omega_G|_{T=\text{const}} = 2.2 \quad (5)$$

and the average value of the derivative of the 2D mode width with respect to the G mode width equals:

$$\partial\Gamma_{2D}/\partial\Gamma_G|_{T=\text{const}} = 0.78 \quad (6)$$

Values displayed in eq. (5) are especially interesting because similar values of the position derivative are attributed to the stress variations within the graphene monolayer [11,49–52]. For instance, Lee [11] claims that "most of pristine graphene sheets exhibit strain in the range of −0.2–0.4%, which varies gradually on the length scale of several microns". As a result, Lee obtained $\partial\hbar\omega_{2D}/\partial\hbar\omega_G = 2.2$, which matches our result exactly. Stress variation can also be observed at the nanometer scale from the analysis of the derivative of the 2D mode width with respect to the G mode width, whose value, according to Neumann [12] and Shin [52], should equal 2.2. In our case, at constant temperature, $\partial\Gamma_{2D}/\partial\Gamma_G = 0.78$, which is significantly below 2.2, taking into account that the diameter of our laser beam is approximately 2 μm, much larger than in the standard case. The conclusion is that the investigated CVD graphene monolayer samples are affected by the stress variation on the length scale of several microns, similar to the graphene samples investigated by Lee and in contrast to the ones examined by Neumann and Shin.

With regard to the mean values of the G and 2D mode positions and widths, there are distinct linear relationships between $\overline{\hbar\omega_G}$ and $\overline{\hbar\omega_{2D}}$ ($\rho \geq 0.99$) and between $\overline{\Gamma_G}$ and $\overline{\Gamma_{2D}}$ ($\rho \geq 0.99$). Therefore, we calculated the derivative of the mean 2D mode position with respect to the mean G mode position, which equals:

$$\partial\overline{\hbar\omega_{2D}}\Big/\partial\overline{\hbar\omega_G} = 2.0\pm0.3 \quad (7)$$

as well as the derivative of the mean 2D mode width with respect to the mean G mode width, which equals:

$$\partial\overline{\Gamma_{2D}}\Big/\partial\overline{\Gamma_G} = 1.7\pm0.8. \quad (8)$$

We note that the relatively high values of both uncertainties come from the high values of the standard deviation of the G and 2D mode positions and widths, in comparison to the changes in the corresponding mean values.

Because the $\partial\overline{\hbar\omega_{2D}}/\partial\overline{\hbar\omega_G}$ value is close to 2.2, we estimate the influence of the stress on the temperature shifts of the Raman mode positions using the following reasoning. First, we assume that the graphene monolayer mimics the thermal expansion of the silicon wafer. The linear thermal expansion coefficient α for silicon equals approximately 2.56×10^{-6} K^{-1}; however, to be precise, we used data from Ref. [53]. The change of stress acting on the graphene monolayer originating from the thermal expansion of the silicon substrate when changing the temperature from 300 K to 500 K equals approximately 0.054%. Assuming, after Shin [52], that $\partial\hbar\omega_G/\partial\varepsilon = -62$ cm^{-1}/% and $\frac{\partial\hbar\omega_{2D}}{\partial\varepsilon} = -138\,\frac{\text{cm}^{-1}}{\%}$, we obtained the contributions of the substrate thermal expansion-induced stress on the derivative of the G and 2D mode positions with respect to the temperature, which equal $\chi_{T,G,Si} = -0.017$ cm^{-1}/K and $\chi_{T,2D,Si} = -0.037$ cm^{-1}/K. Similar values were reported by Calizo for exfoliated graphene on a silicon wafer [15]. This leads to the conclusion that there could be a significant contribution to the Raman peak shifts with temperature from the substrate-induced stress change. Of course, the explanation of the changes in graphene phonon energies with temperature seems to be much more complicated, at least for the reasoning that $\chi_{T,G,HOPG} = -0.011$ cm^{-1}/K for HOPG crystal, which was "attributed to the pure temperature effect without an anharmonic contribution" [54]. We also note that the $\chi_{T,G}$ value for the unstrained HOPG crystal used for mechanical exfoliation in our previous publication [29] is very close to the $\chi_{T,G}$ value for multilayer graphene ($n = 11$) on a Si/SiO$_2$ substrate (see Table 2), suggesting, in contrast, no substrate contribution.

The influence of the substrate expansion on the temperature dependence of the Raman spectra from CVD graphene was first pointed out by Kalbac [25,26,28]. Investigating strain and doping in monolayer and bilayer isotopically labeled graphene Kalbac observed that "in both monolayer and the bottom layer of the bilayer, which are in contact with the substrate, a significant amount of local strain is induced when the temperature is varied. In contrast, the influence of local strain on the top layer is much smaller." These conclusions clearly explain why the values of the derivative of the G and 2D mode positions with respect to temperature for unstrained HOPG sample and for exfoliated multilayer graphene on Si/SiO$_2$ are so close to each other. Moreover, extracted in our previous work [29] value of the interface thermal conductance, much smaller than these reported by other authors [55–59], further proves the claim on the influence of the substrate interaction on χ. The substrate-induced strain was also investigated for CVD graphene on copper foil and glass. For example, Tivanov [60] reported $\chi_G = -0.054 \pm 0.004$ cm^{-1}/K and interpreted this value as significantly higher than the values obtained by other authors due to a volume expansion coefficient difference for graphene and copper foil. However, in this work, we found $\chi_G = -0.051 \pm 0.005$ cm^{-1}/K for CVD graphene on Si/SiO$_2$, which suggests that Tivanov's claim could be premature. Another interesting study of CVD graphene on copper foil was reported by Wang [61], who found $\chi_G = -0.101$ cm^{-1}/K and $\chi_{2D} = -0.180$ cm^{-1}/K. Assuming that the linear thermal expansion coefficient α for copper equals 17×10^{-6} K^{-1}, we obtained $\chi_{T,G,Cu} = -0.105$ cm^{-1}/K and $\chi_{T,2D,Cu} = -0.235$ cm^{-1}/K. We note that the obtained unexpectedly good convergence is puzzling. However, the most striking effect was described by Kolesov [62], who transferred CVD graphene from copper foil onto glass and observed changes in temperature derivative of the G mode position from $\chi_{T,G,Cu} = -0.054$ cm^{-1}/K to $\chi_{T,G,Cu} \approx 0$.

The influence of temperature on phonon properties was analyzed also theoretically. The most interesting is the work of Bonini [63], who found temperature changes in E_{2g} phonon energies both for graphite and graphene, Mounet [64], who found the in-plane coefficient of linear thermal expansion using quasi-harmonic approximation with phonon frequencies and Gruneisen parameters, and Zakharchenko [65] who calculated thermal expansion coefficient using atomistic Monte Carlo simulations. The results obtained in Ref. [63] can be used for the calculation of the graphene thermal expansion coefficient α as described by Yoon [66], Shaina [67], and Tian [68]. In this work, assuming that α is constant in the temperature range of 300 K–500 K, we obtained $\alpha = -2.9 \times 10^{-6}$ K^{-1}, which is a very reasonable value. We note that theoretical predictions on the temperature changes in E_{2g} phonon energy can be easily related to the experimental data because the energy of the double-degenerate E_{2g} phonons taken at the center of the Brillouin zone (Γ point) equals directly the center of the first-order G mode in the Raman spectrum. Unfortunately, in the case of 2D mode [69–71] the situation is far much complicated because physical process underlying emergence of the 2D mode it "is a fourth order process involving four virtual transitions: a laser induced excitation of an electron-hole pair; (ii) electron-phonon scattering with an exchanged momentum **q** close to **K**; (iii) electron-phonon scattering with an exchanged momentum **-q**; (iv)

Table 2
Reported values of temperature coefficients $\chi_{T,G}$ and $\chi_{T,2D}$ in chronological order.

Material	$\chi_{T,G}$ value	$\chi_{T,2D}$ value	Temperature range, atmosphere	Source
EX monolayer	−0.0162 ± 0.0020	–	83 K – 373 K, vacuum	Ref [15]
EX bilayer	−0.0154 ± 0.0006	–	113 K – 373 K, vacuum	
EX monolayer	−0.016 ± 0.002	−0.034 ± 0.004	83 K – 373 K, vacuum	Ref [16]
EX bilayer	−0.015 ± 0.0006	–	113 K – 373 K, vacuum	
X monolayer	−0.0186	–	5 K – 295 K, vacuum	Ref [17]
EX monolayer	−0.035	−0.070	298 – 573, Ar atmosphere	Ref [18]
EX monolayer	−0.019	−0.051	RT – 500 °C, vacuum	Ref [19]
EX monolayer	−0.073 ± 0.008	−0.010 ± 0.01	RT – 515 °C, ambient	Ref [20]
EX monolayer	−0.016	−0.026	77 K – 573 K	Ref [21]
EX monolayer	−0.0468 (T up) 0.0578 (T down)	−0.0946 (T up) 0.0873 (T down)	303 K – 473 K	Ref [22]
EX monolayer	−0.055	−0.085	300 K – 700 K, ambient	Ref [24]
CVD monolayer	−0.0461 ± 0.0056	−0.0662 ± 0.0090	300 – 900 K, He atmosphere	Ref [25]
CVD isotopically labelled bilayer	−0.033 ± 0.001	−0.044 ± 0.003	RT – 1173 K, He atmosphere	Ref [26]
CVD monolayer	−0.024	−0.043	298 K – 673 K, vacuum	Ref [27]
EX multilayer	−0.0168 ± 0.0013	–	300 K – 450 K, ambient	previous work [29]
CVD monolayer	−0.03657*	−0.06829*	473 – 973 K, He atmosphere	Ref [30]
HOPG, unstrained	−0.0169 ± 0.0005	−0.025 ± 0.005 (major) −0.017 ± 0.07 (minor)	300 K – 450 K, ambient	this work
CVD monolayer	−0.051 ± 0.005	−0.101 ± 0.009	300 K – 500 K, ambient	

electron-hole recombination" [69]. Therefore, the Raman 2D peak position and shape result from both phonon and electron band structure. Particularly, the **q** vector, which determines the phonon energy through the $E(\mathbf{q})$ relation depends on the details of the electron band structure.

In Fig. 5, we show the distributions of the derivatives of the G and 2D mode positions with respect to temperature, χ_G and χ_{2D}, and their mutual correlations. We note that the distributions of the derivatives were calculated from the Raman maps acquired for each temperature at the same position of the sample, thus enabling the calculation of the derivative at every point of the specified area. Histograms in Fig. 5a and b comprise all the 'point derivatives' and prove that they follow normal distributions. The mean value of the derivative of the G mode position with respect to temperature equals:

$$\overline{\chi_{T,G}} = \frac{1}{N}\sum_{i=1}^{N}\frac{\partial\hbar\omega_{G,i}}{\partial T} = -0.051\pm0.006\ \mathrm{cm}^{-1}\Big/\mathrm{K} \quad (9)$$

and the mean value of the derivative of the 2D mode position with respect to temperature equals:

$$\overline{\chi_{T,2D}} = \frac{1}{N}\sum_{i=1}^{N}\frac{\partial\hbar\omega_{2D,i}}{\partial T} = -0.101\pm0.011\ \mathrm{cm}^{-1}\Big/\mathrm{K}. \quad (10)$$

The obtained mean values are very close to those calculated using eqs. (1) and (2), including the uncertainties (here, the standard deviations), showing the consistency of our data.

In Fig. 5c, we show the obtained results in the χ_{2D}–χ_G coordinate system supplemented with data from other literature reports, for which the exact numerical values are listed in Table 2. Our results are in good agreement with those reported by other authors and fit well in the overall trend. Moreover, a distinct correlation between χ_G and χ_{2D} can be observed, which is additionally confirmed by the value of the Pearson correlation coefficient of 0.80. The derivative of χ_{2D} with respect to χ_G equals:

$$\partial\chi_{T,2D}\Big/\partial\chi_{T,G} = 1.96. \quad (11)$$

The standard deviation of the data in the direction parallel to the line characterized by parameters obtained with the Deming method equals 0.012 cm^{-1}/K, whereas in the direction perpendicular to that line, the standard deviation equals 0.0034 cm^{-1}/K. The

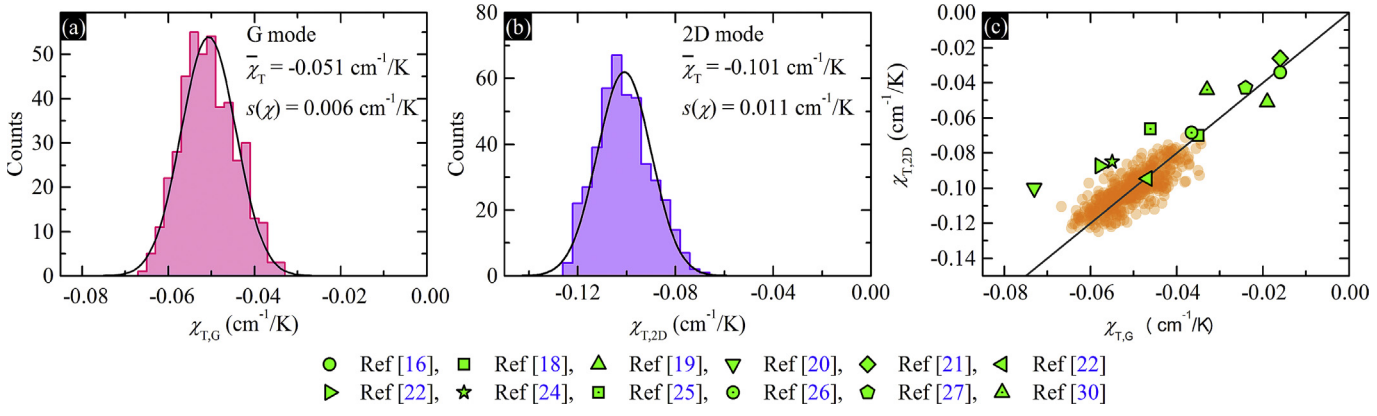

Fig. 5. (a) Histogram of the derivative of the G mode position with respect to the temperature $\partial\omega_G/\partial T = \chi_{T,G}$; (b) histogram of the derivative of the 2D mode position with respect to temperature $\partial\omega_{2D}/\partial T = \chi_{T,2D}$; (c) $\chi_{T,2D}$ versus $\chi_{T,G}$. The gray solid line defines a constant ratio that equals 1.96. (A colour version of this figure can be viewed online.)

Pearson correlation coefficient in the coordinate system based on the directions mentioned above for the data shown in Fig. 5c equals 4×10^{-9}, which should be treated as zero.

The calculated standard deviations of both derivatives illustrate the scope of variation of the investigated parameters within a graphene monolayer sample. This gives a proper outlook on the problem of differences among our and the reference data, which, from this perspective, do not vary much. What is more disturbing is that our values of χ_G and χ_{2D}, and the ones obtained by other authors, seem to be associated. The line with a slope of $\partial\chi_{T,2D}/\partial\chi_{T,G} = 1.96$ well fits not only our results but also those of the others, which clearly suggests that there could be a physical origin of the differences between the χ values, such as doping, stress, the amount of defects or interactions with the substrate. The need for an investigation of this cause is the main conclusion of this work and indicates the direction of possible further research related to the thermal dependence of the phonon properties in graphene and other 2D crystals.

4. Summary

Analysis of the mutual correlations between phonon properties and the comparison to other literature reports led to the conclusion that stress acting on graphene, including that coming from thermal expansion of the substrate, is an important factor when considering the temperature dependence of the phonon energies. The final discussion revealed the existence of an unknown physical cause of differences between reported χ values, demonstrating that the thermal properties of phonons in graphene are still not fully understood and that further studies on the contributions of doping, stress, defects and interactions with the substrate, including its thermal expansion, are required to explain observed divergence in the values of χ_G and χ_{2D} illustrated in Fig. 5c. We also note that the approach presented in this work is not limited to graphene but is universal and can be employed in the investigation of the thermal properties of any other 2D materials or thin films.

5. Notes

The authors declare no competing financial interest.

Acknowledgment

This work was funded by the National Science Centre, Poland, within Project No. 2014/15/D/ST5/03944.

References

[1] A. Reina, X. Jia, J. Ho, D. Nezich, H. Son, V. Bulovic, et al., Large area, few-layer graphene films on arbitrary substrates by chemical vapor deposition, Nano Lett. 9 (2009) 30.
[2] X. Li, W. Cai, J.H. An, S. Kim, J. Nah, D. Yang, et al., Large-area synthesis of high-quality and uniform graphene films on copper foils, Science 324 (2009) 1312.
[3] Z. Yan, Z. Peng, J.M. Tour, Chemical vapor deposition of graphene single crystal, Acc. Chem. Res. 47 (2014) 1327.
[4] T. Ciuk, I. Pasternak, A. Krajewska, J. Sobieski, P. Caban, J. Szmidt, et al., Properties of chemical vapor deposition graphene transferred by high-speed electrochemical delamination, J. Phys. Chem. C 117 (2013) 20833.
[5] Y. Zhang, V.W. Brar, C. Girit, A. Zettl, M.F. Crommie, Origin of spatial charge in homogeneity in graphene, Nat. Phys. 5 (2009) 722.
[6] K.W. Clark, X.-G. Zhang, I.V. Vlassiouk, G. He, R.M. Feenstra, A.-P. Li, Spatially resolved mapping of electrical conductivity across individual domain [grain] Boundaries in graphene, ACS Nano 7 (2013) 7956.
[7] J.D. Buron, F. Pizzocchero, P.U. Jepsen, D.H. Petersen, J.M. Caridad, B.S. Jessen, et al., Graphene mobility mapping, Sci. Rep. 5 (2015) 12305.
[8] Q.H. Wang, Z. Jin, K.K. Kim, A.J. Hilmer, G.L.C. Paulus, C.J. Shih, et al., Understanding and controlling the substrate effect on graphene electron-transfer chemistry via reactivity imprint lithography, Nat. Chem. 4 (2012) 724.
[9] J.M. Englert, P. Vecera, K.C. Knirsch, R.A. Schäfer, F. Hauke, A. Hirsch, Scanning-Raman-Microscopy for the statistical analysis of covalently functionalized graphene, ACS Nano 7 (2013) 5472.
[10] J.D. Wood, G.P. Doidge, E.A. Carrion, J.C. Koepke, J.A. Kaitz, I. Datye, et al., Annealing free, clean graphene transfer using alternative polymer scaffolds, Nanotech 26 (2015), 055302.
[11] J.E. Lee, G. Ahn, J. Shim, Y.S. Lee, S. Ryu, Optical separation of mechanical strain from charge doping in graphene, Nat. Comm. 3 (2012) 1024.
[12] C. Neumann, S. Reichardt, P. Venezuela, M. Drögeler, L. Banszerus, M. Schmitz, et al., Raman spectroscopy as probe of nanometre-scale strain variations in graphene, Nat. Comm. 6 (2015) 8429.
[13] N.J.G. Couto, D. Costanzo, S. Engels, D.-K. Ki, K. Watanabe, T. Taniguchi, et al., Random strain fluctuations as dominant disorder source for high-quality on-substrate graphene devices, Phys. Rev. X 4 (2014) 041019.
[14] L. Banszerus, M. Schmitz, S. Engels, J. Dauber, M. Oellers, F. Haupt, et al., Ultrahigh-mobility graphene devices from chemical vapor deposition on reusable copper, Sci. Adv. 1 (2015) e1500222.
[15] I. Calizo, A.A. Balandin, W. Bao, F. Miao, C.N. Lau, Temperature dependence of the raman spectra of graphene and graphene multilayers, Nano Lett. 7 (2007) 2645.
[16] I. Calizo, F. Miao, W. Bao, C.N. Lau, A.A. Balandin, Variable temperature Raman microscopy as a nanometrology tool for graphene layers and graphene-based devices, Appl. Phys. Lett. 91 (2007) 071913.
[17] L. Zhang, Z. Jia, L. Huang, S. O'Brien, Z. Yu, Low-temperature raman spectroscopy of individual single-wall carbon nanotubes and single-layer graphene, J. Phys. Chem. C 112 (2008) 13893.
[18] D. Abdula, T. Ozel, K. Kang, D.G. Cahill, M. Shim, Environment-induced effects on the temperature dependence of raman spectra of single-layer graphene, J. Phys. Chem. C 112 (2008) 20131.
[19] Z.H. Ni, H.M. Wang, Z.Q. Luo, Y.Y. Wang, T. Yu, Y.H. Wu, et al., The effect of vacuum annealing on graphene, J. Raman Spectrosc. 41 (2010) 479.
[20] L.M. Malard, R.L. Moreira, D.C. Elias, F. Plentz, E.S. Alves, M.A. Pimenta, Thermal enhancement of chemical doping in graphene: a Raman spectroscopy study, J. Phys. Condens Matter 22 (2010) 334202.
[21] D.J. Late, U. Maitra, L.S. Panchakarla, U.V. Waghmare, C.N.R. Rao, Temperature effects on the Raman spectra of graphenes: dependence on the number of layers and doping, J. Phys. Condens Matter 23 (2011) 055303.
[22] H.Q. Zhou, C.Y. Qiu, F. Yu, H.C. Yang, M.J. Chen, L.J. Hu, et al., Raman scattering of monolayer graphene the temperature and oxygen doping effects, J. Phys D Appl Phys 44 (2011) 185404.
[23] K.T. Nguyen, D. Abdula, C.L. Tsai, M. Shim, Temperature and gate voltage dependent Raman spectra of single-layer graphene, ACS Nano 5 (2011) 5273.
[24] C.C. Chen, W. Bao, C.C. Chang, Z. Zhao, C.N. Lau, S.B. Cronin, Raman spectroscopy of substrate-induced compression and substrate doping in thermally cycled graphene, Phys. Rev. B 85 (2012) 035431.
[25] M. Kalbac, O. Frank, L. Kavan, Effects of heat treatment on raman spectra of two-layer 12C/13C graphene, Chem-Eur J. 43 (2012) 13877.
[26] J. Ek-Weis, S. Costa, O. Frank, M. Kalbac, Heating isotopically labeled bernal stacked graphene: a raman spectroscopy study, J. Phys. Chem. Lett. 5 (2014) 549.
[27] N. Hosoya, Y. Akaho, M. Inoue, S. Sahoo, M. Tachibana, Temperature dependence of the Raman spectra of polycrystalline graphene grown by chemical vapor deposition, Appl. Phys. Lett. 105 (2014) 023108.
[28] T.G.A. Verhagen, K. Drogowska, M. Kalbac, J. Vejperova, Temperature-induced strain and doping in monolayer and bilayer isotopically labeled graphene, Phys. Rev. B 92 (2015) 125437.
[29] J. Judek, A.P. Gertych, M. Świniarski, A. Łapińska, A. Dużyńska, M. Zdrojek, High accuracy determination of the thermal properties of supported 2D materials, Sci. Rep. 5 (2015) 12422.
[30] S.D. Costa, J. Ek-Weis, O. Frank, M. Fridrichova, M. Kalbac, Monitoring the doping of graphene on SiO_2/Si substrates during the thermal annealing process, RSC Adv. 6 (2016) 72859.
[31] W. Cai, A.L. Moore, Y. Zhu, X. Li, S. Chen, L. Shi, et al., Thermal transport in suspended and supported monolayer graphene grown by chemical vapor deposition, Nano Lett. 10 (2010) 1645.
[32] A.A. Balandin, Thermal properties of graphene and nanostructured carbon materials, Nat. Mat. 10 (2011) 569.
[33] D.L. Nika, A.A. Balandin, Two-dimensional phonon transport in graphene, J. Phys. Condens Matter 24 (2012) 233203.
[34] D.L. Nika, A.A. Balandin, Phonons and thermal transport in graphene and graphene-based materials, Rep. Prog. Phys. 80 (2017) 036502.
[35] Raman spectra were collected using Renishaw inVia Raman Spectrometer equipped with motorized XYZ stage characterized by 100 nm resolution and Linkam DSC600 optical cell system for the temperature control [according to the specification given by the producer the temperature stability is below 0.1°C]; we used 514 nm Ar laser line, circular polarization [in contrary, e.g., to Ref. 9], Leica microscope, backscattering geometry, grating 600 lines/mm, one spectral window covering G and 2D mode range, 30 seconds acquisition time; calibration was performed using Ne lamp; Lorentzian function with linear background was fitted to every spectrum to get G and 2D mode peak positions, widths [Full Width at Half Maximum – FWHM], and intensities treated in a strict manner as areas, not heights; laser power value was measured using an Ophir Nova II system with photodiode sensor PD-300.
[36] P.S. Peercy, B. Morosin, Pressure and temperature dependences of the raman-active phonons in SnO_2, Phys. Rev. B 7 (1973) 2779.
[37] S. Ryu, L. Liu, S. Berciaud, Y.-J. Yu, H. Liu, P. Kim, et al., Atmospheric oxygen binding and hole doping in deformed graphene on a SiO_2 substrate, Nano Lett.

10 (2010) 4944.
[38] T. Tsukamoto, K. Yamazaki, H. Komurasaki, T. Ogino, Effects of surface chemistry of substrates on raman spectra in graphene, J. Phys. Chem. C 116 (2012) 4732.
[39] A. Favron, E. Gaufrès, F. Fossard, A.-L. Phaneuf-L'Heureux, N.Y.-W. Tang, P.L. Lévesque, et al., Photooxidation and quantum confinement effects in exfoliated black phosphorus, Nat. Mat. 14 (2015) 826.
[40] A. Tiberj, M. Rubio-Roy, M. Paillet, J.-R. Huntzinger, P. Landois, M. Mikolasek, et al., Reversible optical doping of graphene, Sci. Rep. 3 (2013) 2355.
[41] B. Krauss, T. Lohmann, D.-H. Chae, M. Haluska, K. von Klitzing, J.H. Smet, Laser-induced disassembly of a graphene single crystal into a nanocrystalline network, Phys. Rev. B 79 (2009) 165428.
[42] N. Mitoma, R. Nouchi, K. Tanigaki, Photo-oxidation of graphene in the presence of water, J. Phys. Chem. C 117 (2013) 1453.
[43] F. Herziger, R. Mirzayev, E. Poliani, J. Maultzsch, In-situ Raman study of laser-induced graphene oxidation, Phys. Status Solidi B 252 (2015) 2451.
[44] A.E. Islam, S.S. Kim, R. Rao, Y. Ngo, J. Jiang, P. Nikolaev, et al., Photo-thermal oxidation of single layer graphene, RSC Adv. 6 (2016) 42545.
[45] G. Amato, G. Milano, U. Vignolo, E. Vittone, Kinetics of defect formation in chemically vapor deposited [CVD] graphene during laser irradiation: the case of Raman investigation, Nano Res. 8 (2015) 3972.
[46] Evaluation of measurement data — guide to the expression of uncertainty in measurement, in: JCGM 100:2008 GUM 1995 with Minor Corrections.
[47] M. Krystek, M. Anton, A weighted total least-squares algorithm for fitting a straight line, Meas. Sci. Tech. 18 (2007) 3438.
[48] W.E. Deming, Statistical Adjustment of Data, Wiley, NY Dover Publications edition, 1985.
[49] T. Mohiuddin, A. Lombardo, R. Nair, A. Bonetti, G. Savini, R. Jalil, et al., Uniaxial strain in graphene by Raman spectroscopy: G peak splitting, Grüneisen parameters, and sample orientation, Phys. Rev. B 79 (2009) 205433.
[50] M. Mohr, J. Maultzsch, C. Thomsen, Splitting of the Raman 2D band of graphene subjected to strain, Phys. Rev. B 82 (2010) 201409.
[51] Y. Cheng, Z. Zhu, G. Huang, U. Schwingenschlogl, Grüneisen parameter of the G mode of strained monolayer graphene, Phys. Rev. B 83 (2011) 115449.
[52] Y. Shin, M. Lozada-Hidalgo, J.L. Sambricio, I.V. Grigorieva, A.K. Geim, C. Casiraghi, Raman spectroscopy of highly pressurized graphene membranes, Appl. Phys. Lett. 108 (2016) 221907.
[53] T. Middelmann, A. Walkov, G. Bartl, R. Schodel, Thermal expansion coefficient of single-crystal silicon from 7 K to 293 K, Phys. Rev. B 92 (2015) 174113.
[54] P. Tan, Y. Deng, Q. Zhao, W. Cheng, Appl. Phys. Lett. 74 (1999) 1818.
[55] Z. Chen, W. Jang, W. Bao, C.N. Lau, C. Dames, Thermal contact resistance between graphene and silicon dioxide, Appl. Phys. Lett. 95 (2009) 161910.
[56] Y.K. Koh, M.-H. Bae, D.G. Cahill, E. Pop, Nano Lett. 10 (2010) 4363.
[57] K.F. Mak, C.H. Lui, T.F. Heinz, Measurement of the thermal conductance of the graphene/SiO_2 interface, Appl. Phys. Lett. 97 (2010) 221904.
[58] E. Pop, Energy dissipation and transport in nanoscale devices, Nano Res. 3 (2010) 147.
[59] E. Pop, V. Varshney, A.K. Roy, Thermal properties of graphene: fundamentals and applications, MRS Bull. 37 (2012) 1274.
[60] M.S. Tivanov, E.A. Kolesov, A.G. Praneuski, O. Korolik, A.M. Saad, I.V. Komissarov, et al., Significant G peak temperature shift in Raman spectra of graphene on copper, J. Mater Sci. Mater Electron 27 (2016) 8879.
[61] W. Wang, Q. Peng, Y. Dai, Z. Qian, S. Liu, Temperature dependence of Raman spectra of graphene on copper foil substrate, Mater Sci. Mater Electron 27 (2016) 3888.
[62] E.A. Kolesov, M.S. Tivanov, O.V. Korolik, A.M. Saad, Komissarov. Low-temperature anharmonic phonon properties of supported graphene, Carbon 111 (2017) 587.
[63] N. Bonini, M. Lazzeri, N. Marzari, F. Mauri, Phonon anharmonicities in graphite and graphene, Phys. Rev. Lett. 99 (2007) 176802.
[64] N. Mounet, N. Marzari, First-principles determination of the structural, vibrational and thermodynamic properties of diamond, graphite, and derivatives, Phys. Rev. B 71 (2005) 205214.
[65] K.V. Zakharchenko, M.I. Katsnelson, A. Fasolino, Finite temperature lattice properties of graphene beyond the quasiharmonic approximation, Phys. Rev. Lett. 102 (2009) 046808.
[66] D. Yoon, Y.W. Son, H. Cheong, Negative thermal expansion coefficient of graphene measured by Raman spectroscopy, Nano Lett. 11 (2011) 3227.
[67] P.R. Shaina, L. George, V. Yadav, M. Jaiswal, Estimating the thermal expansion coefficient of graphene: the role of graphene-substrate interactions, J. Phys. Condens Matter 28 (2016) 085301.
[68] S. Tian, Y. Yang, Z. Liu, C. Wang, R. Pan, C. Gu, J. Li, Temperature-dependent Raman investigation on suspended graphene: contribution from thermal expansion coefficient mismatch between graphene and substrate, Carbon 104 (2016) 27.
[69] A.C. Ferrari, J.C. Meyer, V. Scardaci, C. Casiraghi, M. Lazzeri, F. Mauri, et al., Raman spectrum of graphene and graphene layers, Phys. Rev. Lett. 97 (2006) 187401.
[70] L.M. Malard, J. Nilsson, D.C. Elias, J.C. Brant, F. Plentz, E.S. Alves, et al., Probing the electronic structure of bilayer graphene by Raman scattering, Phys. Rev. B 76 (2007) 201401.
[71] P. Venezuela, M. Lazzeri, F. Mauri, Theory of double-resonant Raman spectra in graphene: intensity and line shape of defect-induced and two-phonon bands, Phys. Rev. B 84 (2011) 035433.